Journal of Nuclear Materials 385 (2009) 312–318

Contents lists available at ScienceDirect

Journal of Nuclear Materials

journal homepage: www.elsevier.com/locate/jnucmat

Neutron induced damage in reactor pressure vessel steel: An X-ray absorption fine structure study

G. Kuri [a,*], S. Cammelli [a], C. Degueldre [a], J. Bertsch [a], D. Gavillet [b]

[a] LNM, NES, Paul Scherrer Institute, CH-5232 Villigen PSI, Switzerland
[b] AHL, NES, Paul Scherrer Institute, CH-5232 Villigen PSI, Switzerland

ARTICLE INFO

PACS:
61.10.Ht
61.72.Ji
61.80.Jh

ABSTRACT

The radiation damage produced in reactor pressure vessel (RPV) steels during neutron irradiation is a long-standing problem of considerable practical interest. In this study, an extended X-ray absorption fine structure (EXAFS) spectroscopy has been applied at Cu, Ni and Mn K-edges to systematically investigate neutron induced radiation damage to the metal-site *bcc* structure of RPV steels, irradiated with neutrons in the fluence range from 0.85 to 5.0 $\times$ 10^{19} cm^{-2}. An overall similarity of Cu, Ni and Mn atomic environment in the iron matrix is observed. The radial distribution functions (RDFs), derived from EXAFS data have been found to evolve continuously as a function of neutron fluence describing the atomic-scale structural modifications in RPVs by neutron irradiations. From the pristine data, long range order beyond the first- and second-shell is apparent in the RDF spectra. In the irradiated specimens, all near-neighbour peaks are greatly reduced in magnitude, typical of damaged material. Prolonged annealing leads annihilation of point defects to give rise to an increase in the coordination numbers of near-neighbour atomic shells approaching values close to that of non-irradiated material, but does not suppress the formation of nano-sized Cu and/or Ni-rich-precipitates. Total amount of radiation damage under a given irradiation condition has been determined. The average structural parameters estimated from the EXAFS data are presented and discussed.

1. Introduction

The reactor pressure vessel (RPV) is an iron base alloy, and it is the most important pressure-barrier component as far as the safety of a nuclear power plant is concerned. Both neutron irradiation and long term exposure at ~600 K are responsible for the hardening, embrittlement and a decrease in ductility of the RPV steels [1–3]. These are indeed one of the limitations of the lifetime of the reactors. Well-known microstructural changes in the RPV steel under neutron irradiation are irradiation-induced defects, such as vacancies and interstitials, vacancy–impurity complexes of admixture atoms, or a high number density ($\sim 10^{23}$ m^{-3}) of very fine solute clusters [4], the size of which is known to be of the order of few nanometers. Copper is the most important element for clusters formation due to its higher initial (radiation enhanced) diffusivity compared to other solutes. Its solubility in pure Fe at the typical irradiation temperature measures to be also very low (≈0.007% [5]). In practical RPV steels, it is considered that other impurities and alloying elements, for example, P, Mn, Cr, Ni, etc., affect the Cu precipitation process. For the case of low-Cu steels (<0.05%), these solutes can also form precipitates by the same mechanism, causing embrittlement. However, the formation of non-Cu solute precipitates is much slower than for Cu-rich precipitates, and as such the current understanding of such nanostructures on RPV lifetime remains only partially understood [6].

For these reasons, the influence of neutron irradiation in RPV steels has been extensively studied, both theoretically and experimentally, since many years [7–11]. A variety of experimental techniques such as transmission electron microscopy (TEM) [12], field ion microscopy [13], atom-probe topography (APT) [14], positron annihilation [15] and Mössbauer spectroscopy [16], etc. have been used for understanding the defect structures and materials modifications. Beside the mechanical testing commonly used for structural integrity analysis of RPVs, these techniques are applied to provide further sight into the microstructured evolution. However, most of the available experimental data that are used to qualify the various damage models are basically Charpy impact data [8]. The embrittlement is evident from the changes in the mechanical properties of the steels: shift of the ductile-to-brittle transition temperature towards high temperatures, loss of the upper shelf energy and/or reduction of the fracture toughness. It has been also correlated with the neutron flux, total fluence, the temperature and the solute content, especially the amount of P, Mn, Cu and Ni in the

* Corresponding author. Tel.: +41 56 310 2182; fax: +41 56 310 2203.
E-mail address: goutam.kuri@psi.ch (G. Kuri).

0022-3115/$ - see front matter © 2009 Elsevier B.V. All rights reserved.
doi:10.1016/j.jnucmat.2008.12.037

RPV steels. It is now established that the ageing and irradiation related degradation of RPVs are very complex processes dependent on many factors (e.g., irradiation conditions and thermal treatments, chemical compositions, fabrication and post-production processing conditions, etc.). The radiation damage produced, and properties of RPVs strongly depend on its microstructures and testing scenario. Although the basic microscopic mechanisms for the matrix damage accumulation, radiation enhanced solute precipitation and/or grain boundary segregation [9] are fairly well-known, however, due to the complexity of the problem there are still many unknowns regarding migration of solute atoms (Cu, Ni, Mn, etc.) in the presence of defects. Although crystallographic irradiation defects are well visible in TEM as far as they are not single vacancies or interstitials, instead, the created small and coherent precipitates in ferritic steels are very difficult to characterize experimentally. Because of coherency these features are mostly below the resolution limit of the transmission electron microscope. Thus, an atomic-scale description of the lattice disorder in RPV material, which is local in particular and element-specific providing definitive information on the near-neighbour atomic environment, is essential. Local probes that treat ordered and disordered regions on an equal footing should be able to provide a more detailed, atomic-level description of the damage. Nuclear magnetic resonance (NMR) is one such technique, although it does not easily lend itself to a direct structural interpretation. The extended X-ray absorption fine structure (EXAFS) spectroscopy technique employed here provides another local probe. It has the advantage that it gives radial pair-distance distribution information around a specific atomic species, since it relies on the backscattering of a photoelectron from a core excitation. Other experimental methods mentioned above already employed for the description of lattice disorder in in-service RPV steels and/or any iron-based model alloys are not sensitive to any small change in the local, crystallographic next-neighbour atomic distributions.

2. Experimental

2.1. Materials and irradiation

The RPV steels examined were two heats of A533B class 1 plates. The material contains several alloying elements or impurities (1.42% Mn, 0.84% Ni, 0.51% Mo, 0.24% Si, 0.18% C, 0.14% Cu, 0.12% Cr, 0.017% P, 0.004% S and 0.002% V, all in wt% with the balance in Fe). They were prepared for experimental needs during the implementation of an International Atomic Energy Agency (IAEA) co-ordinated research project on the behaviour of RPV steels under neutron irradiation [17]. The neutron irradiation was performed in the 10 MW SAPHIR reactor [at a neutron flux of $\sim 4 \times 10^{12}$ cm^{-2} (fast component >1 MeV)] in Switzerland according to the reactor parameters described in Ref. [18], and at various fluences in the range 0.85—5.0 $\times 10^{19}$ cm^{-2}. The irradiation temperature was controlled at 560 ± 5 K. Thermal annealing (at 735 K for a duration of 168 h) of irradiated samples was conducted in a hot cell under a protective gas atmosphere. Additional specimens were also prepared that were thermally annealed at 735 K for 18 h when 50% of the total target fluence was reached, followed by reirradiation to the same total target fluences. These reirradiation experiments were carried out in the Ford reactor at the University of Michigan in USA. The displacement-per-atom (dpa) parameter was calculated in order to characterize the radiation damage level. For the calculations, the neutron flux spectrum [18] has been used as input to the SPECTER computer code [19]. A simplified calculation gave the dpa doses ranging from 1.2×10^{-2} to 7.1×10^{-2} dpa for 0.85 to 5.0 $\times 10^{19}$ cm^{-2} exposed specimens, respectively, if the threshold energy for Fe displacement is assumed to be 24 eV. However, the helium and hydrogen generation amounts of RPVs were found negligible. Evolution of microstructural features (e.g., ultrafine Cu-, Mn-, Ni-, Si- and P-enriched precipitates etc.) following various stages of irradiation, annealing and/or reirradiation, as well as the mechanical property data of these steels can be found in Refs. [4] and [20]. Four selected samples from this batch were collected for EXAFS measurements the results of which are presented in this work. Details of the specimens are summarized in Table 1. Apart from the irradiated steels, another piece of unirradiated sample (hereafter REF, which was the same material as of the irradiated ones), was also selected for EXAFS investigation.

2.2. EXAFS and data analysis

In order to determine the local atomic configuration of constituent elements in irradiated RPVs, i.e., the nearest-neighbour atomic distance, the relative coordination number, and similar information for some successive shells, we utilized the X-ray absorption spectroscopy (XAS) facility available at the Swiss Light Source (SLS), on the μ-XAS beam line under dedicated ring conditions (2.4 GeV, 400 mA). Due to the high dilution of the samples, all measurements were performed in fluorescence mode using a 32-element hyperpure Ge detector. The incident X-ray intensities were measured by means of a gas-flow ion chamber. Data were also recorded from a pristine RPV specimen (REF) for use as structural comparators and reference spectrum. For calibrating the energy output of liquid nitrogen cooled Si(111) double-crystal Bragg monochromator, the K-edge excitation energy (E_0) of 7112 and 8979 eV measured from high purity iron and copper foils, respectively, were set equal to the maximum of the first derivatives of the absorption spectra. XAS data processing and numerical analysis were performed using the computer program IFEFFIT [21]. Each channel of each scan was examined for glitches prior to averaging. Data reduction was performed in the usual manner, extracting the EXAFS signals $\chi(k)$ after background removal, Fourier transforming (FT) the data in the real space R in order to obtain the radial distribution function (RDF) around the absorber atoms, and back-Fourier transforming in a limited R range, to get first neighbors contribution to the EXAFS signal. As known from the EXAFS theory, the FT reproduces in first approximation the atomic radial distribution function around the probed species (i.e., Cu, Ni and Mn in our case). A quantitative analysis has been done on the FT peaks by using standard fitting procedures. The optimized

Table 1
Neutron irradiations and post-irradiation annealing temperatures for all the samples investigated in the present work.

Specimen identification	1st Irradiation fluence (cm^{-2})	Thermal annealing		2nd Irradiation fluence (cm^{-2})	Thermal annealing	
		T (K)	t (h)		T (K)	t (h)
REF	–	–	–	–	–	–
I	5.0×10^{19}	–	–	–	–	–
IA	5.0×10^{19}	735	168	–	–	–
IAR	0.85×10^{19}	735	18	0.85×10^{19}	–	–
IARA	0.85×10^{19}	735	18	0.85×10^{19}	735	168

structural parameters, namely: S_0^2 - amplitude reduction factor, N – coordination number, R – interatomic distance, σ^2 - Debye Waller (DW) factor, ΔE_0 (a correction to E_0), were derived from the fits, taking into account both the many-electron effects and the vibrations of neighbouring atoms around their equilibrium positions. Quality of the fits were judged by the EXAFS $\Re$-factor as defined in the IFEFFIT code, which represents the absolute misfit between theory and data. The acceptable values are in the order of a few percent with a lower value implying a better fit. Theoretical phase-shift and backscattering amplitude functions for quantitative EXAFS fitting were generated using the modern relativistic code FEFF-8.2 [22]. This theoretical approach describes the photoelectron final states by an ab-initio curved-wave multiple-scattering calculation using an energy-dependent exchange-correlation for self-energy within a muffin-tin potential. In our analysis, K-edges final-state potentials for the central atoms (i.e., Cu, Ni or Mn) were calculated using atomic clusters derived from the known atomic coordinates of body-centered-cubic (*bcc*) phase Fe structures as referred in Refs. [23,24].

3. Results and discussion

3.1. Atomic environment around Cu, Ni and Mn

Examples of measured XAS spectra at the Cu, Ni and Mn K-edges from the reference (i.e., unirradiated, REF) RPV steel sample are shown in Fig. 1. In the inset, magnitude of the corresponding k^3-weighted EXAFS signal is shown. The edge position, taken as equal to the maximum value of the differential coefficients of the spectrum near the edge, reveals an E_0 value of 8979.2, 8333.3 and 6538.6 eV for Cu, Ni and Mn, respectively. These values are indeed identical to the reference K-edge excitation energies of corresponding metal foils. The data presented in Fig. 1 clearly indicate excellent quality EXAFS in the spectral k range of 2—12 $Å^{-1}$ for both Ni and Mn ones, and rather good in the case of Cu although its amount was very low (~0.14 wt%). For a quantitative analysis of these data, the fitting procedure was adopted using the standard methods as summarized in the previous section. Fig. 2 plots Fourier transformed EXAFS spectra for the REF sample as well as that of four neutron-irradiated and annealed RPV steels. In all cases the EXAFS data was weighted by a Hanning window and the range transformed extends from $k = 3.0$ to 10.5 $Å^{-1}$. The spectra drawn with symbols and solid lines are the measured and corresponding best-fitted one, respectively. Table 2 contains the analyzed numerical results for all these specimens. In the insets in Fig. 2(a–c), experimental FT data of all samples for each absorber element are shown in the overlap mode to identify structural differences from a preliminary inspection of the data. It is clear that the observed effects cannot be considered insignificant and/or within the experimental uncertainties.

The EXAFS measurement from the REF steel clearly reveals an excellent crystallinity around all the absorber atoms. The FT data presented in Fig. 2 illustrates Fourier features which are characteristic of the *bcc*-Fe-sites environments. For all three absorber elements (Cu, Ni and Mn) studied the RDF shows that there are three strong amplitude peaks between 2.0 and 5.5 Å whose distance R is around 2.5, 4.0 and 4.8 Å, respectively. A small structure peaking at about 3.4 Å can be also seen in the spectrum. The first strong peak at about 2.5 Å stems from the first and second neighbour of the Fe lattice. The magnitude intensity of the second peak near 4.0 Å is sensitive to the coordination number as well as geometry of third neighbours. The peak around 4.8 Å contains a contribution from long-range order (fourth- and fifth-shell). Information about the local structure in this REF sample is, therefore,

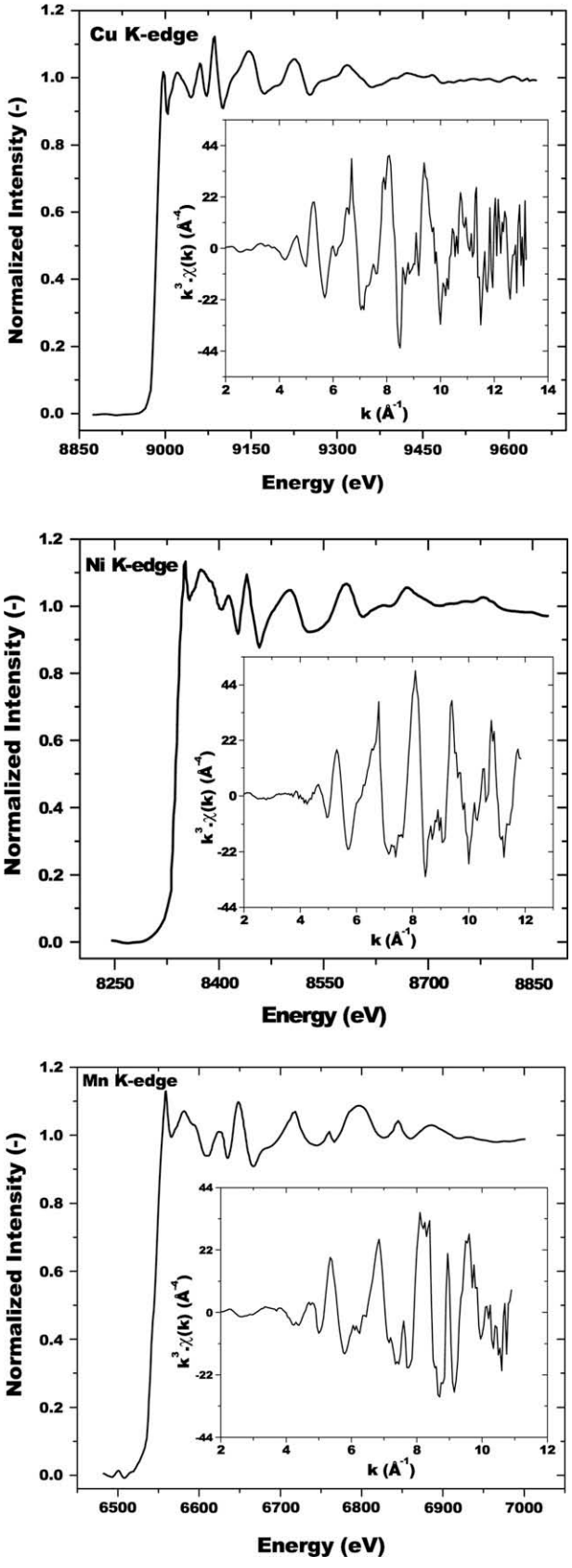

Fig. 1. Normalized and background removed K-edge absorption spectra of pristine RPV steel specimen (REF) in the as-prepared state and before neutron irradiation. The data are shown for Cu, Ni and Mn K-edges. Insets in each plot show the magnitude of the k^3-weighted EXAFS signal versus the photoelectron wave number k.

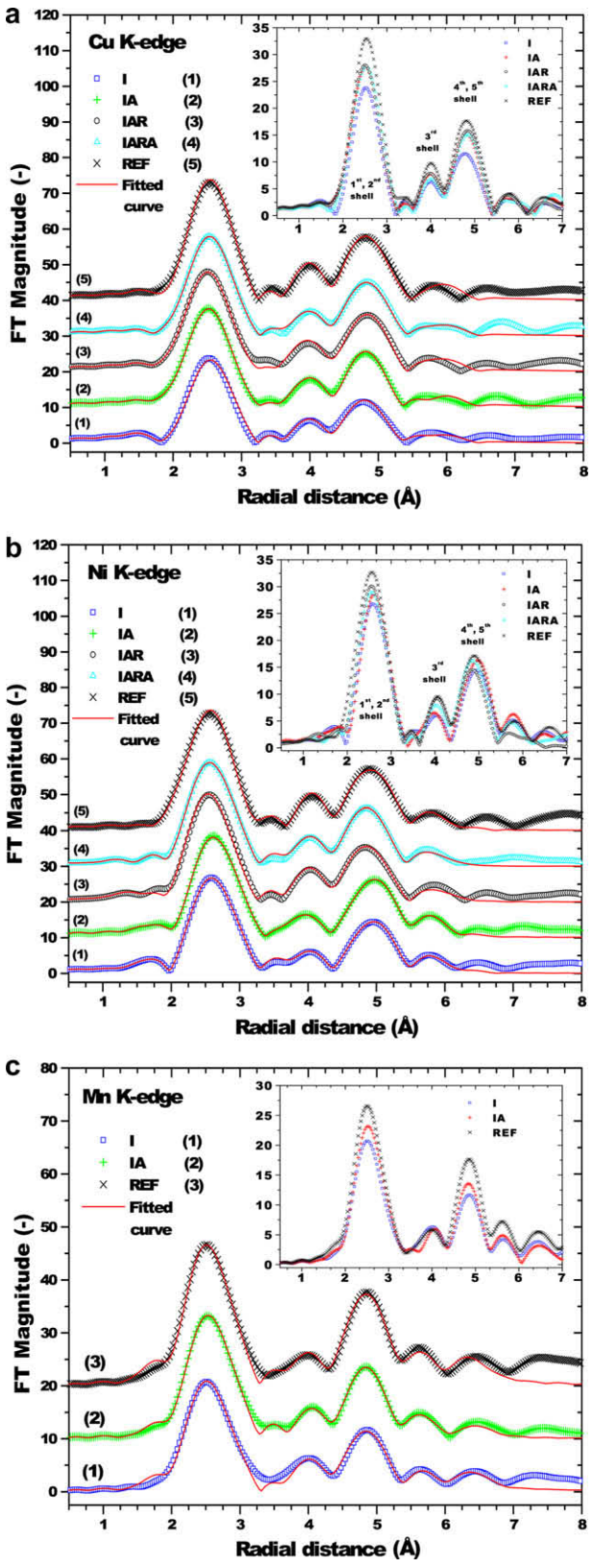

Fig. 2. Fourier transform (FT) of the $k^3 \cdot \chi(k)$ data of the REF sample in Fig. 1 together with the FT data of four neutron irradiated samples as described in Table 1. The Cu edge data (a), Ni edge data (b), and Mn edge data (c) are shown for the transform k range between 3.0 and 10.5 Å^{-1}. In each plot, the curves are vertically shifted with respect to each other for clarity. The data points are provided with symbols and continuous lines represent the best fit to the data. In the insets experimental FT data of all samples are shown in the overlap mode.

obtained by fitting these data with corresponding atomic scattering functions calculated using FEFF [22]. The analysis using FEFF model of the *bcc* Fe lattice structure yielded a good fit to the experimental data. The starting FEFF model comprises all single scattering paths within the fit range and all multiple scattering paths up to 6.0 Å. The single scattering peaks around Cu, Ni and Mn sites are surrounded by 8 Fe atoms at 2.49 Å, 6 at 2.87 Å, 12 at 4.06 Å, 24 at 4.76 Å and 8 at 4.97 Å in the first five consecutive neighbour shells. During the preliminary fitting analysis of Cu, Ni and Mn data of this REF sample, the R, σ^2 and ΔE_0 of contributing atom shells were floated while all other parameters were held fixed at their theoretical values. Once approximate values of the radial distances as well as DW factors were determined, additional fits were carried out in which the R and σ^2 values were fixed and the N, S_0^2 and ΔE_0 values were allowed to vary. Further refinement of the fit was achieved by fixing N, S_0^2, and σ^2 values at the fitted values and again varying R using the previously determined values as the starting values. Finally, all parameters were floated from the starting values determined from the above approach until a best fit for all parameters was obtained. The refined values (see Table 2) obtained from the curve fit give realistic DW factors, correct order for the bonds, and appropriate coordinations for the first five consecutive neighbour shells. All data in Fig. 2 have also been corrected for electron phase shifts using the 1st shell-path from FEFF and therefore the FT peaks should correspond directly with the true bond distances of the near neighbours. At this point let us mention that Cu and Ni atoms, when compared to Fe in terms of their sizes, behave as equivalent backscatterers, and indistinguishable from the XAS point of view. Therefore, in our present analysis, the local environment of solute atoms (i.e., Cu, Ni and even Mn) has been deduced assuming only one kind of neighbour for the central atom residing in a *bcc*-cluster of Fe lattice. Thus, the contributions from Cu–Fe correlation (for example) in the FT peak imply the results of Cu–Fe (Cu,Ni or Mn) atoms-shell in practice, Cu being the central atom.

Dealing with neutron irradiated samples, the RDFs exhibit remarkable differences in many respects. Significant radiation damage effects are readily apparent in the raw data. From the qualitative comparison of RDF spectra of these specimens (shown in Fig. 2) relative to that in the pristine state, following observations can be made. An overall similarity of Cu, Ni and Mn atomic environment in the iron matrix is observed. In the FT data of irradiated samples a systematic attenuation experienced by all peaks corresponding to various next-neighbour shells (first to fifth) is evident. The amplitude reduction is strongest for the specimen irradiated with the highest neutron fluence (sample I), and in the first-FT peak which originates from the first- and second-shell contributions to the FT data. An increase in the EXAFS amplitude can be also observed in the spectrum of the annealed sample irradiated at a neutron fluence of 5.0×10^{19} cm^{-2} with respect to that of the as-irradiated one (I and IA conditions). However, a significantly lesser change is apparent for IAR and IARA samples. In contrast, the peak positions in the RDFs which correspond to metal-metal bond lengths exhibit no neutron-dose or post-irradiation-temperature dependence within experimental error. Preliminary fits to the data from these irradiated samples showed that the decrease in amplitude is due to both a decrease in the amplitude reduction factor S_0^2 and an increase in each atom pair's σ^2 with total neutron fluences. Since the EXAFS amplitude for a given shell is proportional to both N and $1/\sigma$, damping due to disorder results from the disorder-induced increase of the DW factor and the decrease of coordination numbers in each shell. To quantify this damage resulting from neutron irradiation effects, we therefore introduce in our analysis an overall scaling factor (α) multiplied to the term S_0^2. This parameter α should describe the damaged fraction in the irradiated RPV steel lattice. The fits to the EXAFS spectra of irradiated samples were

Table 2
Results of the EXAFS analysis on Cu, Ni and Mn sites in neutron irradiated RPV steels. The EXAFS result of the un-irradiated REF sample is also shown for a comparison. S_0^2 denotes the amplitude reduction factor, α is the scaling factor, and σ^2 represents the Debye Waller factor. See the text for further details.

Absorber atom	Specimens Identification	Overall scaling factor (α)		$\sigma^2(\times 10^{-4})$ (Å^2) (in various coordination shells)			Quality factor $\Re$ (%)
				1st and 2nd	3rd	4th and 5th	
Cu[a]	REF	–	(1.00)	45 (±6)	59	42	1.5
	I	0.73		50	82	63	1.6
	IA	0.80		43	77	46	0.9
	IAR	0.83		46	67	59	1.7
	IARA	0.88		49	82	67	0.3
Ni[a]	REF	–	(1.00)	42	69	109	0.5
	I	0.73		38	79	157	0.7
	IA	0.89		57	65	85	0.5
	IAR	0.92		42	71	85	0.9
	IARA	0.92		42	78	106	0.3
Mn[a]	REF	–	(1.00)	32	68	68	1.4
	I	0.76		36	86	87	1.8
	IA	0.83		29	74	74	1.0

[a] S_0^2, ΔR and ΔE_0 are in the range of 0.83–0.87, −0.08–0.05 Å and −3.0–5.0 eV, respectively.

done in R space. In the fitting procedure the coordination number was fixed to the nominal value for each scattering path. The amplitude reduction factor S_0^2 was also constrained to be the best-fit values of 0.85, 0.83 and 0.87 for Cu, Ni and Mn K-edge data, respectively. These values were derived from the data of REF sample. Special care was taken to extract the high-shell structural information with high accuracy. The data were analyzed in two steps. First, a two-shell fit for the nearest Cu–Fe (also similar for Ni and Mn edge data) coordinations was done in the R range of 1.5–3.5 Å by varying bond lengths R, DW factor, and shift of the energy origin ΔE_0. Second, in the fits for higher shells in the R range from 3.5 to 6.0 Å, σ^2 and R for each path were treated as adjustable parameters, while ΔE_0 was fixed to the best-fit value for the first-two shells. In this way, the correlation between R and ΔE_0 was reduced, and hence the number of free parameters in the fits. This approximation is reasonable, since Cu (or Ni) and Fe have the similarity in their ionic radii, and have very close values of electronegativity [25]. Therefore, the electrostatic potentials induced by charge transfer between Cu and Fe atoms can be neglected, and the approximation of neutral absorber atom assumed by FEFF is valid, so that an overall ΔE_0 is enough for all scattering events. The overall fitting results are shown in Fig. 2 as continuous lines superimposed on the data points. The best-fit structural parameters are summarized in Table 2. The values for interatomic distances R are not mentioned in Table 2 as they were found not being affected by the neutron irradiations and within the experimental uncertainties.

Considering the information derived from EXAFS analyses following conclusions can be drawn from Table 2. The main difference in the local structural parameters due to irradiations is a systematic change in overall scaling factor α that relates changes in the coordination numbers in nearest-neighbour atomic shells, and an increase in the DW factors upon irradiation and post-irradiation annealing. These results are not graphically depicted since they are also partly evident in the RDFs spectra shown in Fig. 2 (see the insets). The progressive decrease of the nearest-neighbour peak-amplitude is indicative of an increase in the number of displaced atoms (point defects) in the vicinity of the absorbing atoms, produced by a primary knock-on atom (PKA) with a given kinetic energy. During prolonged neutron irradiations the creation of these primary point defects (in terms of vacancies and interstitials atom) is extremely high, and they also have a much higher probability of reacting with themselves. This means, in the case of an interstitial and a vacancy reaction simply results in annihilation but in the case of vacancies can result in the production of the di-vacancy or higher order vacancy complexes. To relax the anisotropy of the corresponding lattice distortion short range (dis)ordering of the neighbouring ion vacancies can also occur. These would in turn result in the decrease in volume for the surroundings of Cu, Ni or Mn, which contributes to the relaxation of the lattice distortion derived from the local strain field. Therefore, it is reasonable to consider that the decrease in the coordination numbers in next-neighbour shells upon irradiation is caused, at least partly, by simple point defects and/or their agglomerates associated with each of the constituent solute atoms in RPV steel. Upon post-irradiation-annealing at higher temperatures, the vacancy- and interstitial-like defects that do not recombine may, respectively, preferentially diffuse to voidlike sinks and self-anneal through bond rearrangements with nearest neighbors. A reduced fraction of defects will thus retain within the bulk. During formation of these defects, copper together with other alloying elements leads to precipitation of nano-precipitates, and also induces matrix hardening and embrittlement. This precipitation effect is expected to saturate due to the progressive reduction of available precipitable elements in solid solution, copper in particular. Furthermore, other light elements, like phosphorus or sulphur, can segregate inside the grains interacting with matrix defects (i.e., vacancies, interstitials, dislocation loops), or migrate to grain boundaries, or may be attracted to the Cu-type precipitates. Diffusion of segregates also plays a role.

One can furthermore note from Table 2 that changes in σ^2, or equivalently, the mean-square relative displacement of the interatomic distance distribution, is more pronounced in the higher-shells (third to fifth). Apparent changes upon relaxations observed in σ^2 for the first two shells are not significant in the irradiated samples relative to the REF sample, yielding an average value of 0.0046, 0.0044 and 0.0032 Å^2 for the Cu, Ni and Mn atomic neighbours, respectively. In contrast, σ^2 is increased from 0.0059 to 0.0082 Å^2 in the third shell in high fluence 5.0×10^{19} cm^{-2} sample, with a significantly lesser change apparent due to post-irradiation annealing. Similar behaviour can be also observed for the lowest dose IAR and IARA samples. These trends remain consistent in the measured σ^2 data of fourth- and fifth-shells neighbours. In all cases of the annealed specimens the structures are not well-ordered beyond the first two coordination shells. The fact that the local *bcc* structure around Cu and Ni atoms is almost the same in IAR and IARA specimens suggests that the initial sample structure remains preserved by the modification induced by neutron irradiations and post-irradiation annealing process; the only difference evidenced by the EXAFS analysis is about the Debye Waller factor that is lower in the case of IAR than in IARA, indicating in this last case a more disordered local structure. It appears that additional

defect complexes, mostly small and well separated, are formed around Cu and Ni atoms in the matrix upon annealing.

While it is difficult to propose a unique structural model accounting the actual lattice positions of all Cu, Ni and Mn atoms in Fe, and it is highly probable that in these irradiated steels Cu, Ni and Mn are present in a number of different local configurations (e.g., strained and/or distorted lattice positions, ultrafine clusters in a *bcc* environment etc.), the following remarks may be relevant in connections with our results obtained from EXAFS experiments. The accumulated damage after irradiation in sample I is measured as about 26% from the point of view of each of the constituent solute atoms in RPV steel. This amount of radiation damage is obtained from the value of α, which was found to decrease greatly on irradiation, that is from 1.0 to 0.74 (an average value calculated from the Cu, Ni and Mn data) in this sample. Thermal annealing at 735 K for a duration of 168 h induces a local ordering and improves the crystallinity in this sample as manifested by a reduced damage fraction close to 16%. The estimated damage in the lowest dose IAR and IARA (measured only at the Cu and Ni K-edges) samples vary between 10% and 12%. These values of the retained damage are not directly correlated with the *dpa* parameter that we have mentioned earlier for characterizing the radiation damage level in these samples. The matrix damage enhancement, while possibly indicating more defects than expected, may also indicate significantly more defect-induced lattice strain and distortions. Therefore, it is important to mention that the matrix damage reported here should be interpreted as a collection of surviving point defect clusters resulting from vacancies and self-interstitial atoms, loops and nanovoids, as evolved with temperature and time, and interacting with solute atoms and elements of the microstructure to promote formation and growth of the mentioned nanoscale features [4,26].

3.2. Atomic environment around Fe

In the following we present the Fe K-edge EXAFS results obtained for the high fluence I and IA specimens. The results are shown in Fig. 3. The upper panel in the figure reports Fe K-edge XAS spectra. The lower panel plots FT data and the best-fitted curves. The EXAFS oscillations (inset in Fig 3(a)) and the corresponding FT (inset in Fig 3(b)) of I sample have similarities with those of IA specimen. Prolonged annealing after the neutron irradiation shows no influence on the Fe first- and second-nearest neighbour shells, although a small change in the higher order shells (third to fifth) of iron can be observed. Also, the Fe environment, reflected in both oscillation and FT data from the REF sample (not shown here), is very similar to the results presented in Fig. 3. Results of the first coordination shell fitting parameters obtained for I sample are: an Fe–Fe coordination number of 7.5 ± 0.3 at a distance 2.52 ± 0.02 Å, $\sigma^2 = (59 \pm 7) \times 10^{-4}$ Å^2 and $\Delta E_0 =$ 9.6 eV; whereas the corresponding values for the second shell are $N = 6.6 \pm 0.3$, $R = 2.89 \pm 0.02$ Å, $\sigma^2 = (59 \pm 7) \times 10^{-4}$ Å^2 and $\Delta E_0 = 9.6$ eV. The estimated errors are the standard ones for EXAFS. These values are in agreement with the parameters known in the literature [23] for a *bcc* unit-cell of an Fe lattice. Describing the situation for the annealed one (IA specimen), the best fit is obtained with similar values for first two shells. The main structural difference between the two samples is the Debye Waller factors of higher order shells. For the third shell we measure $\sigma^2 = (77 \pm 6) \times 10^{-4}$ Å^2 in sample I, and in IA $\sigma^2 = (69 \pm 5) \times 10^{-4}$ Å^2. Theoretical FEFF calculations [22] incorporating an in-plane statistical disorder in the atomic layers of a *bcc* (100) structure and accounting multiple scattering contributions to the EXAFS-FT third shell peak indicate the expected larger value of σ^2 observed for this shell. These results are not presented here, and will be published separately. In fact, from the data measured at the Fe K-edge and their analyses, no essential structural changes in the first two near-neighbour

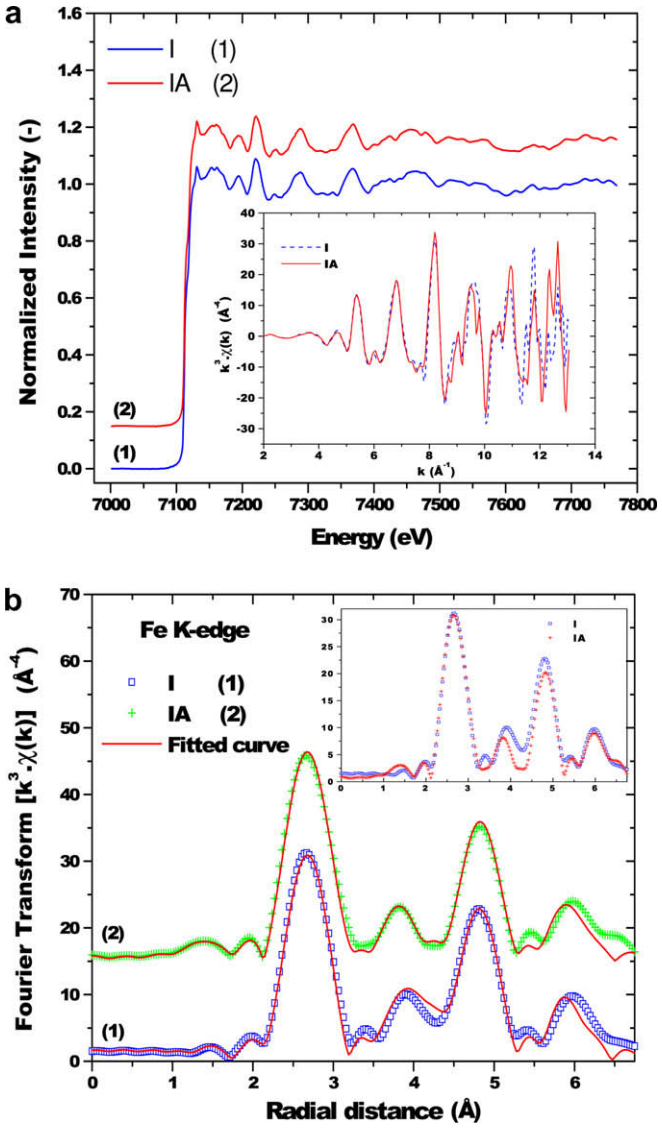

Fig. 3. (a) The XAS spectra at the Fe K-edge after background subtraction from a 5.0×10^{19} cm^{-2} sample in the as-irradiated state and after thermal annealing (735 K for 168 h), I and IA conditions, respectively. The inset shows k^3-weighted EXAFS oscillations. (b) Corresponding radial distribution functions (Phase-shift corrected) around Fe atoms as Fourier transforms of the *k*-spectra. In the inset experimental FT data of these two samples are shown in the overlap mode. See the text for details.

shells are observed between the REF and irradiated steel specimen. However, this is not the case for that of the Cu, Ni and Mn neighbours indicative of more specific vacancy type defect environments in close proximity to these solute atoms. It is noteworthy that XAS is more sensitive to defect environment close to impurity sites (Cu, Ni and Mn) in comparison to their bulk (Fe) counterpart. The lack of the observation of intensity decrease in Fe-EXAFS signal could partly originate also from a different vacancies to the number of atoms ratio in alloying elements with respect to pure iron. Nevertheless, following few remarks may be relevant in connection with the results obtained here. In recent years, several studies of defect evolution in irradiated Fe and Fe–Cu alloys from atomistic simulations have been undertaken describing the role of intracascade point defects clustering including correlated recombination [27,28], defect transport properties [29], and binding as well as stability of vacancy-solute clusters [30]. Representative experimental study [31] of Fe irradiated at 310 K by neutrons showed consistent

results in that almost all the microstructures resolved by the TEM technique were interstitial type dislocation loops, and no vacancy-type defect was observed. Vacancies introduced by cascades in the Fe lattice form clusters by primarily agglomerating in small regions, but such formed clusters are not stable at temperatures that is close to the RPV operation temperature of 563 K. Specific computer simulations of the cascade and defect microstructure evolution have predicted results also in the same direction: the size and fraction of self-interstitial atoms clusters are larger in Cu than in Fe [32]. The vacancies on the other hand, are in Cu mostly in the form of clusters, while they do not cluster in Fe [33].

4. Conclusions

In this work, structural characterization of a reactor pressure vessel (RPV) IAEA reference steel samples irradiated with neutrons has been performed through EXAFS spectroscopy studies. The EXAFS technique is sensitive to the atomic environment only few atoms away from the probe and provides measures of the short range order ($\sim$1 nm) of the system. Selected RPV steel specimens bombarded with neutrons at nuclear power plants with in-service reactor operating conditions, and in the fluence range of $0.85–5.0 \times 10^{19}$ cm^{-2} have been identified for the investigations. Thermal annealing was also conducted on a few selected specimens to study the thermal stability of defects developed by neutron irradiation. EXAFS spectra performed at the K-edge of Cu, Ni and Mn show that these atoms reside in a closed-packed arrangement similar to that of *bcc* Fe. A quantitative analysis has been done by analyzing the Fourier-transformed EXAFS data, and adopting a best-fit simulation procedure in order to determine the near-neighbour atomic environment around these absorber atoms. The main difference in the local structural parameters due to irradiations is a systematic change in the coordination numbers in nearest-neighbour atomic shells, and an increase in the Debye Waller (DW) factor upon irradiation and post-irradiation annealing. Such changes in the coordination numbers are however not apparent in the EXAFS data measured at the Fe K-edge; here only a slight increase in the DW factor is observed from the data analysis. The results are attributed to the involvement of point defects and their equilibrium population in the vicinity of these absorber elements. These results trigger further experimental work as well as theoretical model calculations for the atomic-scale description of lattice damage to clarify their possible influence on technological applications of neutron irradiation into RPV material.

Acknowledgement

The authors gratefully acknowledge the μ-XAS beam-line staff for the experimental work performed at SLS. Our sincere thanks are to Swissnuclear for financially supporting this work.

References

[1] G.R. Odette, G.E. Lucas, Radiat. Eff. Defects Solids 144 (1998) 189.
[2] K. Fukuya, K. Ohno, H. Nakata, S. Dumbill, J.M. Hyde, J. Nucl. Mater. 312 (2003) 163.
[3] E. Vincent, C.S. Becquart, C. Pareige, P. Pareige, C. Domain, J. Nucl. Mater. 373 (2008) 387.
[4] See for example: S. Cammelli, C. Degueldre, G. Kuri, J. Bertsch, Nucl. Instr. Meth. Phys. Res. B 266 (2008) 4775. and references therein.
[5] S. Miloudi, Etude du Dommage d'Irradiation dans les Aciers de Cuve des Réacteurs à Eau Pressurisée, PhD Thesis, Université d'Orsay, 1997.
[6] A. Zeman, L. Debarberis, L. Kupča, B. Acosta, M. Kytka, J. Degmová, J. Nucl. Mater. 360 (2007) 272.
[7] G.R. Odette, G.E. Lucas, J. Am. Soc. Test. Mater. STP 909 (1986) 206.
[8] R. Chaouadi, R. Gérard, J. Nucl. Mater. 345 (2005) 65.
[9] M.K. Miller, P. Pareige, M.G. Burke, Mater. Charact. 44 (2000) 235.
[10] M.K. Miller, M.G. Burke, J. Nucl. Mater. 195 (1992) 68.
[11] J.Z. Liu, A. van de Walle, G. Ghosh, M. Asta, Phys. Rev. B 72 (2005) 144109. and references therein.
[12] R. Monzena, K. Takadaa, K. Matsudab, Z. Metallkund. 11 (2003) 1241;
E.A. Kuleshova, B.A. Gurovich, Ya I. Shtrombakh, D.Yu. Erak, O.V. Lavrenchuk, J. Nucl. Mater. 300 (2002) 127.
[13] M.K. Miller, K.F. Russell, P. Pareige, M.J. Starink, R.C. Thomson, Mater. Sci. Eng. A 250 (1998) 49.
[14] D. Blavette, F. Vurpillot, P. Pareige, A. Menand, Ultramicroscopy 89 (2001) 145;
M.K. Miller, R.K. Nanstad, M.A. Sokolov, K.F. Russell, J. Nucl. Mater. 351 (2006) 216.
[15] V. Slugeň, A. Zeman, M. Petriska, V. Kršjak, Appl. Surf. Sci. 252 (2006) 3309.
[16] V. Slugeň, A. Zeman, J. Lipka, L. Debarberis, NDT&E Int. 37 (2004) 651.
[17] Reference Manual on the IAEA JRQ Correlation Monitor Steel for Irradiation Damage Studies, IAEA-TECDOC-1230.
[18] W.B. Waeber, D.H. Njo, J. Am. Soc. Test. Mater. STP 1011 (1989) 48;
E. Lehmann, Ergebnisse von Reaktorphysikalischen Untersuchungen für den Kern des Forschungsreaktors SAPHIR unter Verwendung des Programmsystems ELCOS, TM-41-94-10, Paul Scherrer Institute, 1994.
[19] L.R. Greenwood, R.K. Smither, SPECTER: Neutron Damage Calculations for Materials Irradiations, ANL/FPP/TM-197, Argonne National Laboratory, 1985.
[20] R.K. Nanstad, M. Niffenegger, R.D. Kalkhof, M.K. Miller, M.A. Sokolov, Ph. Tipping, J. Am. Soc. Test. Mater. STP 1475 (2006) 195;
M. Niffenegger, K. Reichlin, D. Kalkhof, Nucl. Eng. Des. 235 (2005) 1777.
[21] <http://cars9.uchicago.edu/ifeffit/feffit.html>.
[22] J.J. Rehr, J.M.d. Leon, S.I. Zabinsky, R.C. Albers, J. Am. Chem. Soc. 113 (1991) 5135. version 8.20 used.
[23] V.G. Harris, K.M. Kemner, B.N. Das, N.C. Koon, A.E. Ehrlich, J.P. Kirkland, J.C. Woicik, P. Crespo, A. Hernando, A.G. Escorial, Phys. Rev. B 54 (1996) 6929.
[24] G. Kuri, C. Degueldre, J. Bertsch, J. Rothe, J. Nucl. Mater. 362 (2007) 274.
[25] J.A. Alonso, L.A. Girifalco, Phys. Rev. B 19 (1979) 3889.
[26] Q. Xu, T. Yoshiie, K. Sato, Philos. Mag. Lett. 87 (2007) 65;
Q. Xu, T. Yoshiie, K. Sato, Philos. Mag. Lett. 88 (2008) 353.
[27] C.J. Ortiz, M.J. Caturla, Phys. Rev. B 75 (2007) 184101.
[28] A.C. Arokiam, A.V. Barashev, D.J. Bacon, Yu.N. Osetsky, Phys. Rev. B 71 (2005) 174205.
[29] J. Marian, B.D. Wirth, A. Caro, B. Sadigh, G.R. Odette, J.M. Perlado, T. Diaz de la Rubia, Phys. Rev. B 65 (2002) 144102. and references therein.
[30] A. Takahashi, N. Soneda, S. Ishino, G. Yagawa, Phys. Rev. B 67 (2003) 024104.
[31] M. Victoria, N. Baluc, C. Bailat, Y. Dai, M.I. Luppo, R. Schaublin, B.N. Singh, J. Nucl. Mater. 276 (2000) 114.
[32] W.J. Pythian, R.E. Stoller, A.J.E. Foreman, A.F. Calder, D.J. Bacon, J. Nucl. Mater. 223 (1995) 245.
[33] M.J. Caturla, N. Soneda, E. Alonso, B.D. Wirth, T. Diaz de la Rubia, J.M. Perlado, J. Nucl. Mater. 276 (2000) 13.